City Research Online

City, University of London Institutional Repository

This is the accepted version of the paper.

This version of the publication may differ from the final published version.

Design and modelling of dispersion engineered all-chalcogenide triangular core fiber for mid-infrared region supercontinuum generation

M. R. Karim[1], H. Ahmad[1,*], and B. M. A. Rahman[2]

[1] *Photonics Research Centre, University of Malaya, 50603 Kuala Lumpur, Malaysia*
[2] *Department of Electrical and Electronic Engineering, City University of London, Northampton Square, London, EC1V 0HB, UK*
[*] *Corresponding author: harith@um.edu.my*

An ultrabroadband mid-infrared supercontinuum (SC) source has been designed and modelled using a 10-mm-long all-chalcogenide triangular core fiber (TCF). The TCF structure can be fabricated from $Ge_{11.5}As_{24}Se_{64.5}$ chalcogenide glass as a core and $Ge_{11.5}As_{24}S_{64.5}$ chalcogenide glass for its cladding running along the length of the fiber instead of air-holes. Assuming the pump operates at 4 μm, the TCF is optimized by varying its side length both anomalous and all-normal dispersion SC generation. Mid-infrared region SC spectral broadening spanning beyond 15 μm could be generated with a low peak power of 3 kW by the proposed TCF structure optimized with varying its side length between 7 and 8 μm in anomalous dispersion pumping. On the other hand, the TCF side length has to be decreased to 5.5 μm and below to optimize it for pumping in all-normal dispersion region SC generation. A coherent flat-top SC evolution in the mid-infrared region of up to 7 μm could be observed by this design with the same pump peak power and pulse duration applied before. The ultrawide optical bandwidth obtained by the proposed TCF design can be an effective tool for mid-infrared region applications such as optical coherence tomography, molecular fingerprint spectroscopy and biomedical imaging. © 2017 Optical Society of America

OCIS codes: *(000.4430) Numerical approximation and analysis; (190.0190) Nonlinear optics; (230.7370) Dispersion; ((060.4005) Microstructured fiber; (160.4330)Nonlinear optical materials; (320.6629) Supercontinuum generation.*

http://dx.doi.org/10.1364/ao.XX.XXXXXX

INTRODUCTION

Supercontinuum (SC) generation in the mid-infrared (MIR) (2–20 μm) region particularly is of high interest owing to the fundamental vibrational absorption of most molecules located in this spectral region . Although the atmospheric transparency is better in the two spectral windows of 3–5 μm and 8–13 μm, however, the second window sees great importance in molecular fingerprint spectroscopy as well as used to detect trace-gas in a variety of industrial and atmospheric applications [1]. Until recently, as the fiber based geometries have higher design flexibilities to achieve desirable dispersion properties through the engineering their structural parameters, optical step-index fibers as well as microstructured based fibers made of highly nonlinear materials are used to generate ultrabroadband MIR SC evolution in the long wavelength region [2, 3]. Chalcogenide materials are very interesting and promising materials containing high intrinsic Kerr nonlinearity with a wide transmission window in the MIR region making them more suitable for the fabrication of

microstructured and step-index fibers that can be employed to generate ultrabroadband MIR SC evolutions exceeding 15 μm [4–7]. Microstructured fibers can be fabricated by employing a single material as a core and air-holes running along the entire length of the fiber as a cladding or a combination of materials with the core and cladding being made from two different materials [8, 9].

Recently, the generation of various ultrabroadband SC spectra in the MIR region has been demonstrated both experimentally [5, 10–18, 31–35] and numerically [19–23, 36]. Petersen *et al.* experimentally demonstrated the MIR SC spectra up to 13.3 μm with a step-index fiber made from $As_{40}Se_{60}/Ge_{10}As_{23.5}Se_{66.6}$ ChG glass and pumped with 100-fs pulse duration at 6.3 μm with a peak power of 2.29 MW [10]. Cheng *et al.* reported a MIR SC spectrum covering a wavelength range of 2-15.1 μm in a 3-cm-long $As_2Se_3/AsSe_2$ ChG step-index fiber pumped with 170-fs pulses in 9.8 μm with a peak power of 2.89 MW [5]. Zhao *et al.* experimentally reported the MIR SC

generation spectra spanning from 2 μm to 16 μm using 14-cm-long tellurite glass (Ge-Te-AgI) step-index fiber pumped at 7 μm with a 150-fs pulse width having a repetition rate of 1 kHz with a pump peak power of 77 MW in the normal dispersion regime [11]. Petersen *et al.* experimentally demonstrates a broadband MIR SC generation spectra covering from 1 to 11.5 μm with high average output power above 4.5 μm in tapered large-mode-area chalcogenide $Ge_{11}As_{22}Se_{68}$ photonic crystal fiber [12]. Hudson *et al.* reported a broadband MIR SC spectrum spanning from 1.8 to 9.5 μm using As_2Se_3/As_2S_3 tapered fiber by launching 230-fs pulses with a pulse peak power of 4.2 kW [13].

Møller *et al.* reported a MIR SC spanning the wavelength range 1.7 to 7.5 μm with an 18-cm suspended core $As_{38}Se_{62}$ fiber having core diameter of 4.5 μm by using pump at 4.5 μm with a pump peak power of 5.2 kW [14]. Zhao *et al.* experimentally demonstrated a MIR SC generation covering the wavelength range 1.5 to 14 μm by a 23-cm Te-based ChG step-index fiber pumped at 4.5 μm with a pulse duration of 150-fs [16]. Yu *et al.* demonstrated a MIR SC generation spanning from 1.8 to 10 μm by pumping an 11-cm-long step-index ChG fiber with 330-fs pulses at 4 μm with a low peak power of 3 kW [17]. Kubat *et al.* numerically shows the MIR SC generation extending up to 12.5 μm by using ChG step-index fiber made employing AsSe as a core and GeAsSe as a outer cladding pumped at 4.5 μm with a peak power of 4.7 kW [19]. In our previous microstructured fiber based designs [23], three different designs were reported namely the triangular core fiber (TCF), hexagonal photonic crystal fiber (H-PCF) and equiangular spiral photonic crystal fiber (ES-PCF). These were designed by microstructuring the cladding through the incorporation of air holes into the cladding for ultrabroadband SC generation in the MIR region. An ultrabroadband MIR SC spectrum spanned up to 11 μm using an ES-PCF pumped at 3.1 μm with 3 kW of input power. Due to the nature of the group velocity dispersion (GVD) parameter at this pump wavelength, however, the SC spectrum could not be extended beyond 6 μm using the TCF design. In this work, a 10-mm-long all-chalcogenide TCF microstructured fiber geometry made employing $Ge_{11.5}As_{24}Se_{64.5}$ glass as its core and $Ge_{11.5}As_{24}S_{64.5}$ glass employed as its cladding instead of air-holes running along the length of the fiber is numerically designed for investigating the MIR SC evolutions between the anomalous and all-normal dispersion regimes. The core of this TCF fiber has been designed with an equilateral triangle of having equal side length suspended by three struts of 0.2 μm thick at the three corner of the fiber and this can be easily fabricated by using extrusion technique [29]. Typical triangular core fiber is made of suspended core type, however, in case of our design dispersion of the TCF fiber can be easily controlled by making the triangular core smaller/larger with reducing/increasing the side length of the fiber. Moreover, a TCF core can be much smaller than that of a hexagonal PCF and other typical microstructured fibers due to stronger index contrast and better control of its structural parameters which eventually results better confinement yielding high nonlinear interaction. Depending on the compositions, ChG glass can be transparent beyond 15 μm in the MIR region and the glass compositions made of GeAsSe/GeAsS, which are chosen for our TCF design, have been used to fabricate waveguides and different step-index as well as microstructured fibers for SC generation successfully [15, 24, 27, 39].

Initially, three different designs are optimized for pumping in the anomalous dispersion region by varying the TCF side length between 7 μm and 8 μm. It is possible to predict an ultrabroadband SC extending into the MIR region up to 16 μm
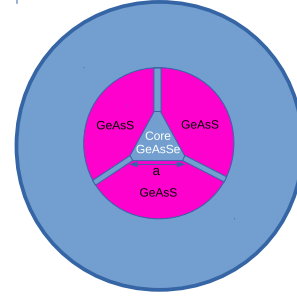

Fig. 1. Triangular core fiber geometry

with a low input peak power of 3 kW by one of the proposed TCF design with a side length of 8 μm. Subsequently, the side length of the TCF geometry is reduced gradually to obtain the GVD parameter for pumping the structure in an all-normal dispersion profile. An all-normal dispersion design is obtained for a side length of 5.5 μm and below, and above that value the design remains in anomalous dispersion regime. By varying side length from 5.5 to 4.5 μm, three designs for all-normal dispersion SC generation are optimized. Inducing a minor spectral fluctuation around the pump wavelength, a broadband coherent MIR SC spectrum could be obtained spanning up to 7 μm with a TCF side length of 5.5 μm. Spectral fluctuation could significantly be reduced by lowering the side length to 4.5 μm by keeping the same pump pulse and power applied before. However, the SC bandwidth decreases slightly at the TCF output owing to its side length reduction, which eventually increases the spectral flatness around the pump wavelength.

Table 1. Sellmeier coefficients

Material	GeAsSe[24]		GeAsS[24]	
m	2		2	
	A_j	λ_j	A_j	λ_j
$j = 1$	5.78525	0.28795	4.18011	0.31679
$j = 2$	0.39705	30.39338	0.35895	22.77018

THEORY

The cross-section of the proposed TCF structure is shown in Fig. 1. During waveguide simulation, the linear refractive index of $Ge_{11.5}As_{24}Se_{64.5}$ and $Ge_{11.5}As_{24}S_{64.5}$ ChG glasses has been calculated using the Sellmeier equation [24],

$$n(\lambda) = \sqrt{1 + \sum_{j=1}^{m} \frac{A_j\lambda^2}{\lambda^2 - \lambda_j^2}},$$ **(1)**

where λ denotes the wavelength in micrometers. The values of Sellmeier fitting coefficients are given in Table 1.

In computational photonics, finite-element is a very powerful and well established numerical tool for characterizing an optical waveguide with any refractive index distribution. We employ our in-house finite-element based full vectorial mode-solver (FEM) to calculate mode effective index ($n_{eff} = \lambda\beta(\omega)/2\pi$) of the fundamental mode (H_x^{11}) of the proposed TCF structure

up to the wavelength range of interest. The FEM is based upon dividing the waveguide region into a large number of non-overlapping triangular elements. We represent our TCF structure with 500,000 first-order triangular elements (500 × 500 mesh) across the transverse dimensions. The field over each element is then expressed in terms of polynomials weighted by the fields over each element. By differentiating the functional with respect to each nodal value, the problem is reduced to a standard eigenvalue matrix equation, which is solved to obtain the propagation constants $\beta(\omega)$ and associated field profiles of various quasi-TE and quasi-TM modes. In the full-vectorial formulation one needs to minimize the full $\mathbf{H}$-field energy functional using [25],

$$\omega^2 = \frac{\iint \left[(\nabla \times \mathbf{H})^*.\hat{\varepsilon}^{-1}(\nabla \times \mathbf{H}) + p(\nabla.\mathbf{H})^*(\nabla.\mathbf{H}) \right] dxdy}{\iint \mathbf{H}^*.\hat{\mu}\mathbf{H}\, dxdy}, \quad (2)$$

where $\mathbf{H}$ is the vectorial magnetic field, * denotes a complex conjugate and transpose, ω is the angular frequency, p is a weighting factor for the penalty term to eliminate spurious modes, and $\hat{\epsilon}$ and $\hat{\mu}$ are the permittivity and permeability tensors, respectively. To calculate the confinement losses, perfectly matched layer (PML) is used to truncate the computational domain. Later, modal solution accuracy was tested by a powerful extrapolation technique called Aitken's extrapolation through convergence between the raw FEM results and extrapolated values with respect to the increased number of mesh elements [41].

On the other hand, the GVD is an another important waveguide characterizing parameter which can be evaluated from n_{eff} obtained by the FEM solver using the following GVD equation [26]

$$\text{GVD}(\lambda) = -\frac{\lambda}{c} \frac{d^2 \text{Re}(n_{\text{eff}})}{d\lambda^2}, \quad (3)$$

where c denotes the speed of light in the vacuum.

To study the MIR SC generation both in the anomalous and all-normal GVD regions, the optical pulse evolution inside the optimized TCF structure is modeled by solving the one-dimensional generalized nonlinear Schrödinger equation (GNLSE) [26]:

$$\frac{\partial}{\partial z} A(z,T) + \frac{\alpha}{2} A - \sum_{r \geq 2}^{14} \frac{i^{r+1}}{r!} \beta_r \frac{\partial^r A}{\partial T^r}$$

$$= i \left(\gamma + i\frac{\alpha_2}{2A_{\text{eff}}} \right) \left(1 + \frac{i}{\omega_0} \frac{\partial}{\partial T} \right)$$

$$\times \left(A(z,T) \int_{-\infty}^{\infty} R(T) \mid A(z, T - T') \mid^2 dT' \right), \quad (4)$$

Here $A(z,T)$ indicates the slowly varying pulse envelop evolving along the length of TCF structure in a retarded time frame with reference $T = t - \beta_1 z$ moving at the group velocity $v_g = 1/\beta_1$, β_r ($r \geq 2$) is the second and higher-order dispersion terms expanded by Taylor-series expansion from the mode propagation constant $\beta(\omega)$ around the center angular frequency ω_0 and α is the linear attenuation (propagation loss) of the TCF. γ is the nonlinear parameter defined as $\gamma(\omega_0) = n_2\omega_0/(cA_{\text{eff}})$, where n_2 is the nonlinear refractive index, $A_{\text{eff}} = (\iint |E|^2 dxdy)^2/(\iint |E|^4 dxdy)$ is the mode effective area of the fundamental mode of TCF structure at the pump wavelength, and the two-photon absorption coefficient is expressed by $\alpha_2 = 7.88 \times 10^{-14}$ m/W [30], however, it can be assumed negligible at a wavelength of 4 μm. The total nonlinear response function $R(t)$ is expressed as

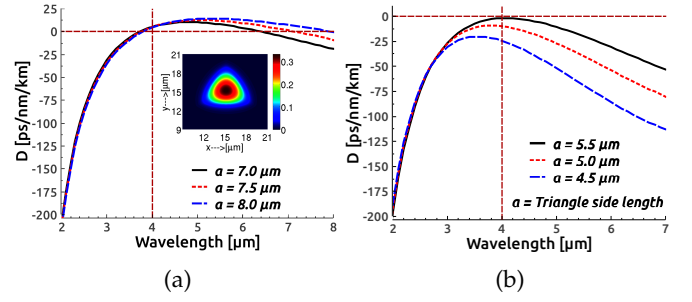$$R(t) = (1 - f_R)\delta(t) + f_R h_R(t), \quad (5)$$

Fig. 2. GVD curves optimized for the TCF geometry shown in Fig. 1 with the variation of its side length a for pump employing in (a) anomalous dispersion region and (b) normal dispersion region. The inset of Fig. 2(a) shows the fundamental mode profile (H_x^{11}) for the TCF structure of side length containing 8 μm at pump wavelength. The vertical dashed line indicates pump wavelength.

Here, $\delta(t)$ is the instantaneous Kerr response and $h_R(t)$ is the delayed Raman response expressed as

$$h_R(t) = \frac{\tau_1^2 + \tau_2^2}{\tau_1 \tau_2^2} \exp\left(-\frac{t}{\tau_2}\right) \sin\left(\frac{t}{\tau_1}\right), \quad (6)$$

where the response function coefficients of chalcogenide material are predicted as $f_R = 0.148$, $\tau_1 = 23$-fs and $\tau_2 = 164.5$-fs which are the Raman coefficients of a single-peak Lorentz function fitted to the As_2Se_3 chalcogenide material [33, 37] as the actual values of f_R, τ_1, τ_2 for the ternary GeAsSe chalcogenide materials not yet reported.

The coherence of the SC spectra obtained in the all-normal dispersion region for the proposed TCF can be tested from numerical simulations by generating an ensemble average of independent SC pairs $[E_1(\lambda), E_2(\lambda)]$ with different random noise seeds. Thus, the complex degree of first-order coherence $|g_{12}^{(1)}(\lambda)|$ can be defined as [38]

$$|g_{12}^{(1)}(\lambda)| = \frac{\langle E_1^*(\lambda) E_2(\lambda) \rangle}{\sqrt{\langle |E_1(\lambda)|^2 \rangle \langle |E_2(\lambda)|^2 \rangle}}. \quad (7)$$

where the angular brackets denote an ensemble average of independently generated SC spectra pairs.

DISPERSION ENGINEERING OF TCF

SC spectral evolution at the optical waveguide output significantly depends on GVD optimization. The GVD of the optical
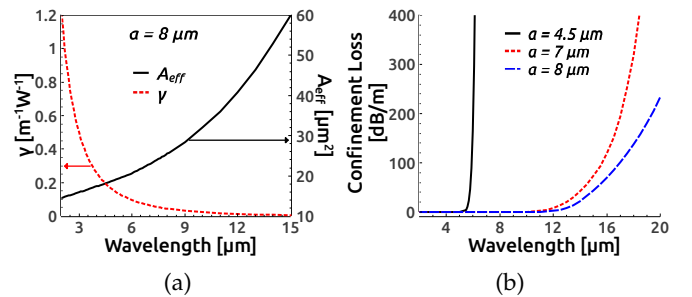

Fig. 3. (a) Mode effective areas and their corresponding nonlinearities over wide wavelength range for the TCF structure of containing side length 8 μm. (b) Confinement losses are calculated for the TCF side length of 4.5, 7 and 8 μm.
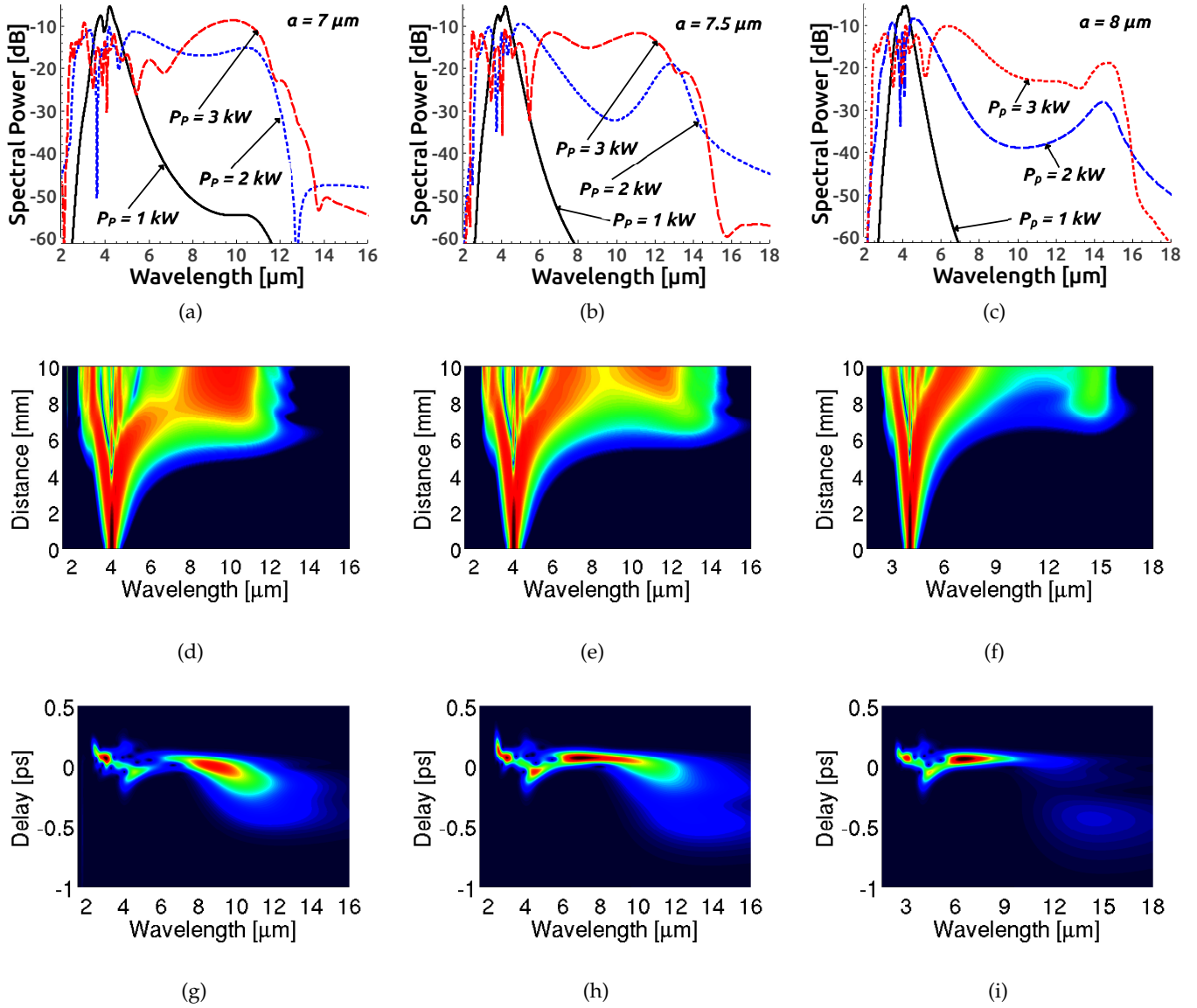
3

Fig. 4. Anomalous dispersion SC spectra (top row), spectral density (middle row) and spectrogram (bottom row) represent the TCF structure with triangle side length of 7 μm (left column), 7.5 μm (middle column) and 8 μm (right column), respectively.

waveguide can be tailored to pump the waveguide in either the all-normal dispersion or anomalous dispersion regions. To extend the SC into the MIR region, pump wavelength requires to be shifted to a longer wavelength depending on the availability of such a pump source in that region. To obtain SC spanning far into the MIR, our proposed TCF geometry is optimized for pumping in both dispersion regions assuming the pump wavelength at 4 μm by varying its structural parameter side length, a. To obtain suitable GVD curves both in the anomalous and all-normal dispersion regimes for pumping at this wavelength, numerous FEM modal solutions are performed on the proposed triangular-core structure with the variation of its side length keeping the thickness of all three struts are constant at 0.2 μm (each strut) placing at the three corners of a TCF structure to obtain mode effective index over a wide range of wavelengths. Our design shows a slight birefringence and we obtain mode effective index of both fundamental H_x^{11} (slow axis) and H_y^{11} (fast axis) modes. The GVD parameters are calculated up to the wavelength range of interest from the mode effective index ob-

tained by the FEM mode-solver for both polarizations but shows very little difference between them. Among the numerous GVD curve variations obtained, two sets of GVD curves are shown for the fundamental mode (H_x^{11}) of TCF structure in Fig. 2. These GVD curves are optimized for pumping both in the anomalous and all-normal GVD regions varying TCF side length from 8 μm to 4.5 μm. The GVD curves shown in Fig. 2(a) are tailored for simulating SC generation in anomalous dispersion pumping by varying the side length in the range, $a = 7 - 8$ μm. To obtain all-normal dispersion GVD curves, the TCF side length, a is reduced to 5.5 μm and below. Fig. 2(b) shows the second set of GVD curves optimized for all-normal dispersion pumping with the variation of side length, $a = 5.5 - 4.5$ μm.

SC GENERATION IN THE MIR REGION

SC simulations are carried out by solving GNLSE Eq. (4) through symmetrized split-step Fourier method by MATLAB for observing MIR SC spectral broadening in the optimized TCF designs

in both the anomalous and all-normal dispersion regimes. Numerical simulations were carried out by taking 2^{17} number of grid points with a minimum temporal resolution of 6.67-fs so that time window can accommodate extreme spectral broadening inside it by avoiding negative frequency generation. The number of axial steps in pulse propagation direction are taken as 100,000 with a step size of 0.1 μm.

SC generation in anomalous dispersion pumping

The damage threshold of ChG glasses needs to be considered before SC generation. Among different composition of ChG glasses, GeAsSe based composition has the lowest damage threshold which is an average power density of 30 kW/cm^2. However, the damage threshold of Sulphide (S) based ChG materials is more than selenium (Se) based compositions. The ChG fiber core could be damaged if the peak intensity of pump pulses reaches 30 GW/cm^2, or the average power density at the input facet of the fiber exceeds 100 kW/cm^2. Paying attention to these factors, we have designed our TCF fiber for MIR SC generation such that the required peak power of pump pulses is 3 kW or lower [17].

For predicting the MIR SC spectral evolution in anomalous dispersion region pumping, a secant pulse of 100-fs full-width at half maximum (FWHM) duration has been propagated in an optimized 10-mm-long TCF structure at a pump wavelength of 4 μm with input peak power variation between 1 and 3 kW. Before SC simulation, the FEM mode-solver is used to calculate A_{eff} = 13.10 μm^2, 14.57 μm^2 and 16.14 μm^2 at pump frequency for the TCF cross-section of side lengths 7 μm, 7.5 μm and 8 μm, respectively. Using these A_{eff} values, the nonlinear coefficient γ can be calculated as 0.34 /W/m, 0.31 /W/m and 0.28 /W/m for the proposed TCF geometries. Frequency dependent nonlinear coefficients, which are illustrated in Fig. 3(a), can be calculated from the mode effective areas obtained over wide wavelength range for a TCF side length of 8 μm. During nonlinear coefficient calculation, the nonlinear refractive index n_2 has been reduced to 1/3 times at 4 μm from the measured value of 7.33×10^{-18} m^2/W at 1.55 μm [30]. The GVD values for the three designs are calculated as 5.17 ps/nm/km, 4.99 ps/nm/km and 4.33 /ps/nm/km, respectively. The linear fiber propagation loss is considered to be 0.5 dB/cm at a pump wavelength during all SC simulations both in the anomalous and all-normal dispersion regimes though the loss may assume to be negligible in such a short fiber design [39]. The confinement losses of TCF side lengths of 4.5 μm, 7 μm and 8 μm are shown in Fig. 3(b). The tunable soliton pump source, which can be tuned between 2 and 4.3 μm with a pulse duration of 100-fs [40], is employed during all SC simulations. In our previous study [41], we found that there is a possibility to obtain spurious results due to inclusion of insufficient number of higher-order GVD terms during the SC simulations. To avoid spurious results as well as to obtain more accurate SC spectral evolution at the TCF output, higher-order dispersion terms up to 14$^{\text{th}}$ order are included during all numerical simulations.

Figure 4 shows the anomalous dispersion SC spectral broadening with a peak power variation between 1 and 3 kW spanning the spectrum far into the MIR region. By rigorous numerical simulations, it is determined that an ultrabroadband SC spectra can be realized with the proposed three dispersion engineered all-chalcogenide TCF designs in the MIR region covering the wavelength ranges 2.2–13.5 μm, 2.3–15 μm and 2.3–16 μm as shown in Figs. 4(a), 4(b) and 4(c), respectively with a low input peak power of 3 kW. In all cases, the SC bandwidths are mea-
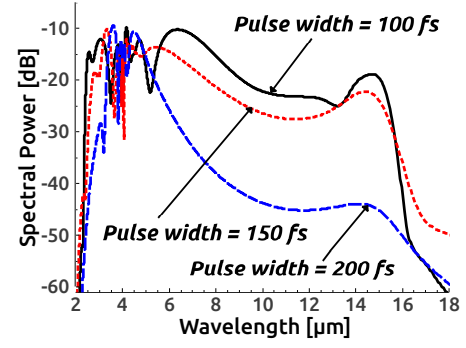

Fig. 5. The output SC spectra obtained with the variation of pulse duration for the TCF structure of side length having 8 μm with a largest peak power of 3 kW.

sured in -30 dB level from the peak. According to the dispersion length, $L_D = T_P^2/|\beta_2|$ and the nonlinear length, $L_{\text{NL}} = 1/\gamma P$, the soliton order, $N = \sqrt{L_D/L_{\text{NL}}}$ can be calculated as 8.66, 8.35 and 8.53 and the soliton fission occurs approximately in 5 mm distance for the three TCF structures with the side lengths of 7 μm, 7.5 μm and 8 μm, respectively. Relatively small anomalous GVD as well as lower GVD slopes over the wide wavelength range (which can be seen in Fig. 2(a)) help to produce large Raman induced frequency shifts by forming the Raman soliton inside the TCF structure. Moreover, a large red shifted dispersive wave (DW) induced due to the suppression of Raman induced frequency shift after the second ZDW of each TCF design. The spectral density evolutions (middle row) and spectrograms (bottom row) in Fig. 4 for the three proposed TCF designs exhibit fission process which is initiated approximately at a distance of 5 mm of each geometry produces multiple fundamental solitons whose spectrum shifts toward the stokes-side (long wavelength region) due to Raman induced frequency shift which eventually yields a number of spectral peaks in the spectra. Due to spectral recoil effect, it can be seen from the Fig. 4 (middle and bottom rows) that solitonic propagations stop at the second zero dispersion wavelengths (ZDWs) at around 6.4 μm, 7.2 μm and 7.9 μm for the three TCF structures with a side length of 7 μm, 7.5 μm and 8 μm, respectively. A strong and large red shifted DW, owing to the presence of higher-order dispersion terms, emits in the long wavelength side by the fundamental solitons where energy transfer occurs from solitons to DW in the form of nonsolitonic radiation as can be seen in the Fig 4. It is also appeared that a DW is produced at a wavelength before the first ZDW of the
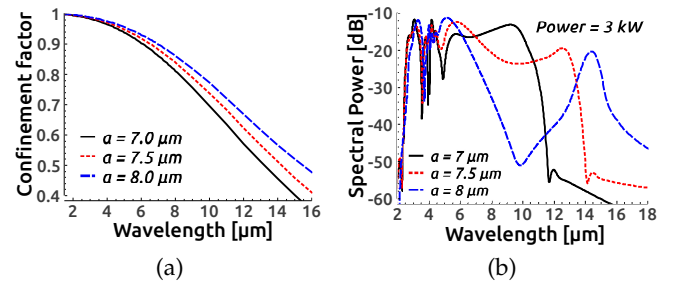

Fig. 6. (a) The confinement factor (power in core/total input power) and (b) the SC output spectra considering 2.5 dB linear loss during simulations for the TCF structure of containing side length between 7 and 8 μm.
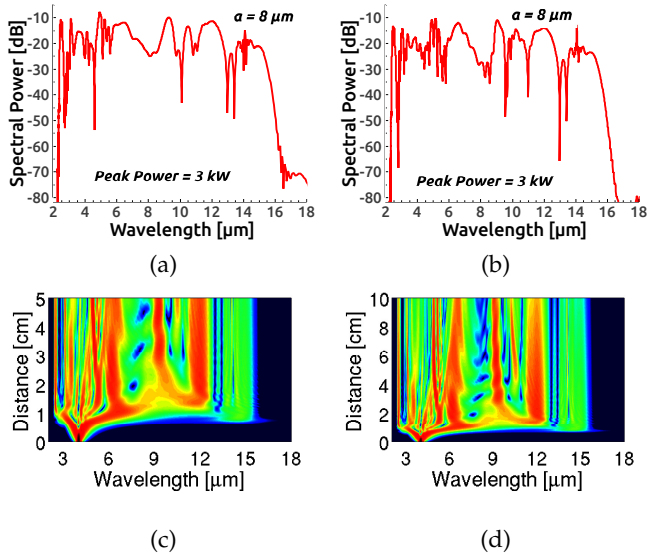
(a)

(b)

(c)

(d)

Fig. 7. The SC output spectra after the pulse propagation of (a) 5-cm, (b) 10-cm and their corresponding spectral density after (c) 5-cm, (d) 10-cm of propagation for the TCF structure of side length having 8 μm.

fiber falling in the normal dispersion region by the all proposed anomalous dispersion TCF designs. By varying pulse width between 100 and 200-fs, we have also performed numerical simulations for the TCF structure of side length containing 8 μm with same peak power applied before and the resulting output SC spectra illustrated in Fig. 5.

Until to date the highest MIR SC spectrum experimentally reported by Cheng *et al.* [5] spanning in the range of 2-15.1 μm in a 3-cm-long ChG step-index fiber (As$_2$Se$_3$/AsSe$_2$) pumped at 9.8 μm with a peak power of 2.89 MW. On the other hand, the highest SC expansion by numerical simulation was reported by Saini *et al.* [21] covering the wavelength range 2-15 μm in a 5-mm long triangular core graded index As$_2$Se$_3$ photonic crystal fiber pumped at 4.1 μm with a largest peak power of 3.5 kW. However, by our proposed TCF design, it is possible to obtain SC broadening in the MIR region up to 16 μm pumped at 4 μm with a lower peak power of 3 kW. Actual experimental situation will be different from numerical case as more pump peak power will be required to compensate coupling loss between pump source and TCF structure to obtain identical SC bandwidth in experimental condition.

Among ChG glass compositions, sulphide (S) based ChG glass has high absorption loss beyond 10 μm wavelength. Since our proposed TCF structure is designed employing GeAsS glass as an outer cladding, definitely this design would show high absorption loss beyond the 10 μm of SC extension. To quantify this loss problem, we have calculated the confinement factor of the fundamental mode, H$_x^{11}$ for our proposed TCF design containing side lengths between 7 and 8 μm which is shown Fig. 6(a). It can be observed from figure that fundamental mode of our TCF design carries 40, 46 and 52 percent of total applied power through fiber core at a wavelength of 15 μm by the structure containing the side length of 7, 7.5 and 8 μm, respectively. On the other hand, 48 percent of total input power is retained inside the core of TCF containing side length 8 μm at a wavelength of 16 μm. As the core still carries large portion of input power beyond 10 μm, the SC extension beyond this wavelength could
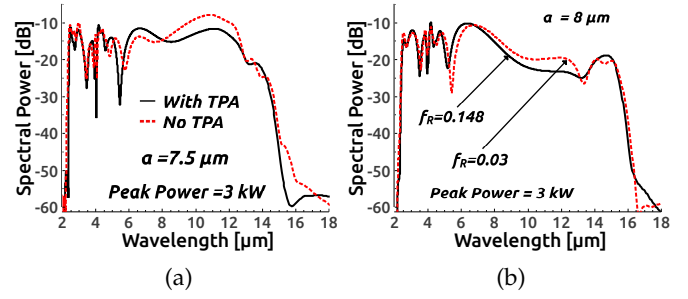

(a)

(b)

Fig. 8. The comparison of SC output spectrum (a) with and without TPA; (b) using single and dual peak Lorentz function values.

be broadened by core power carrying through the fundamental mode of a TCF design. Since we could not able to obtain the long wavelength absorption edge of core/cladding materials, further SC simulations were carried out to predict the effect of cladding absorption in long wavelength region for the proposed structures by increasing linear loss from 0.5 dB/cm to 2.5 dB/cm which is assumed arbitrarily based on confinement factor obtained in Fig. 6(a). Although the output SC spectrum containing TCF side length of 8 μm in Fig. 6(b) shows a deep dip induced at the middle of the spectrum as a result of high loss, the output spectra of the other two geometries demonstrated in the figure still could be the encouraging predictions by our designs.

To minimize losses, we propose a short length TCF which is 10-mm long. As per as loss concerned, TCF length can be increased and we have shown in Fig. 7 the obtained results by simulating 5 and 10-cm long two TCF structures. It can be observed from Figs. 7(a) and 7(b) that SC bandwidth remains almost same at TCF output and further SC broadening stops after 1-cm of propagation and only the smoothening of the spectrum takes place up to remaining length of propagation which are shown in Figs. 7(c) and 7(d), respectively. We have carried out further SC simulations for a single input pulse to test the impact of TPA on obtainable SC bandwidth at the TCF output. We have noticed only negligible impact of TPA on output SC bandwidth which is shown in Fig. 8(a). Throughout in all our SC simulations we use single peak AsSe Lorentz function which is different from dual peak Raman frequency response induced by GeAsSe ternary ChG materials. We obtain SC spectrum by setting up fractional Raman response value f$_R$ = 0.03 in numerical simulations which was considered by Petersen *et al.* [12] for their recent MIR SC demonstration by tapered photonic crystal fiber made with ternary GeAsSe ChG material. The output SC spectrum obtained between fractional Raman response value of 0.03 and 0.148, which are shown in Fig. 8(b), does not make any significant difference on SC bandwidth though a minor spectral changes observe between 7 and 13 μm, however, the average power of the two spectrum are same at the TCF output.

SC generation in all-normal dispersion pumping

SC generation in the all-normal dispersion region is less popular than SC generation in the anomalous dispersion regime as more SC broadening can be obtained in anomalous dispersion pumping due to solitonic propagation inside the optical waveguide. However, smooth and flat as well as highly coherent SC spectra with moderate bandwidth can be obtained by normal dispersion pumping [42–47]. In all-normal dispersion pumping, no solitonic propagation occurs as the SC extends only due to
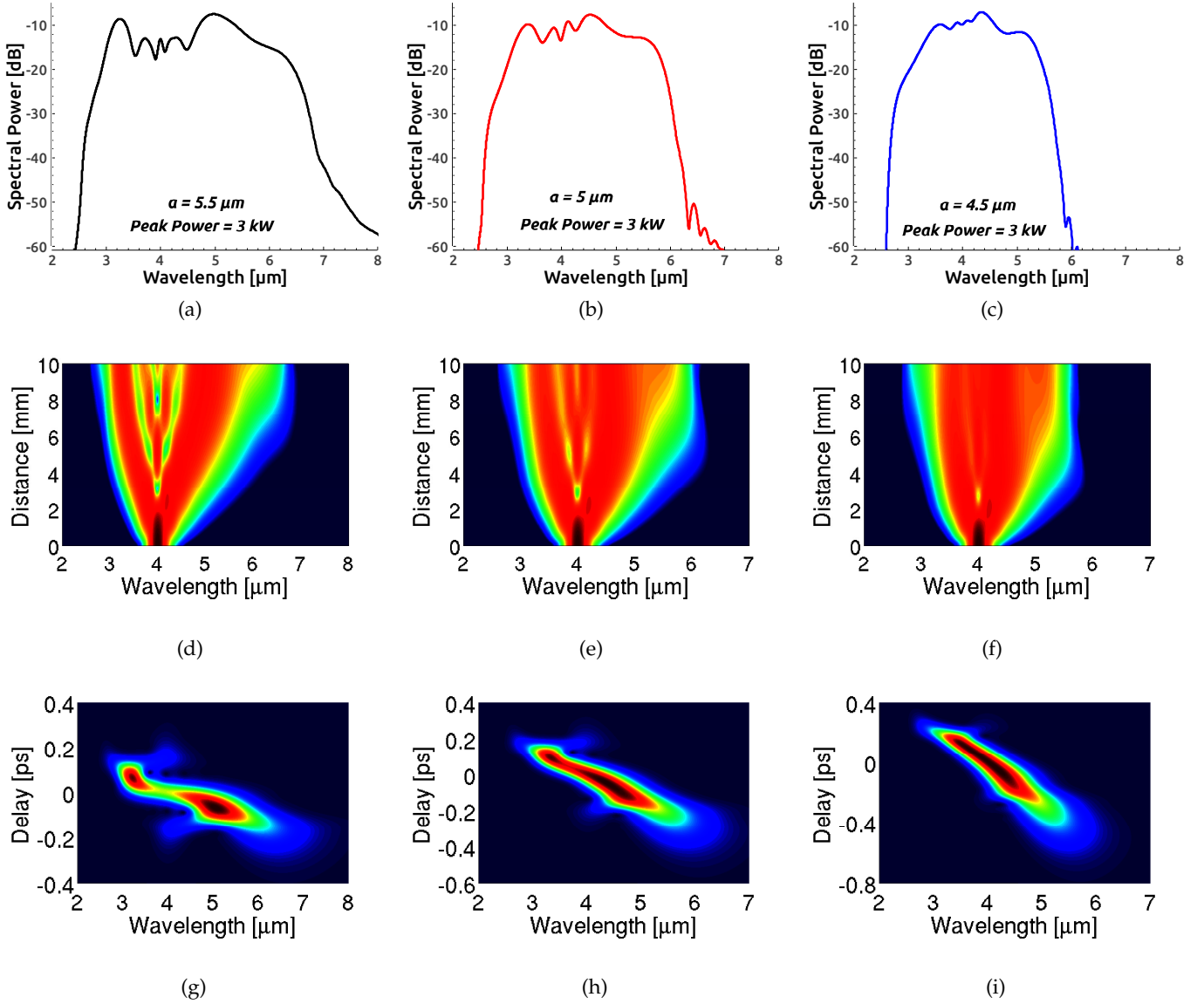
Fig. 9. All-normal dispersion SC spectra(top row), spectral density (middle row), spectrogram (bottom row) represent the TCF structure with triangle side length of 5.5 μm (left column), 5 μm (middle column) and 4.5 μm (right column), respectively.

self-phase modulation (SPM) and optical wave breaking (OWB). Since no soliton are induced in normal dispersion pumping which limits the spectral broadening, resulting in more flatness in the output SC spectrum that can be highly suitable for precision measurement applications. The pump pulse duration is an another important factor acting in spectral fluctuation reduction and typically pump pulse width should keep less than 100-fs in duration during all-normal dispersion SC generation.

To obtain a smooth and flat MIR SC spectra in all-normal dispersion region, three different TCF structures are engineered with the variation of side length between 5.5 μm and 4.5 μm. The same pump source with the equal power is employed in normal GVD pumping SC generation. Before simulations, the mode effective areas, A_{eff} = 9.24 μm^2, 8.16 μm^2 and 7.2 μm^2 are evaluated by the FEM mode-solver for the three designs whose GVD curves are shown in Fig. 2(b). The nonlinear coefficients are calculated as γ = 0.44 /W/m, 0.5 /W/m, 0.56 /W/m at 4 μm at a wavelength of 4 μm. At this wavelength, the GVD parameters for three different designs are calculated as -1.79 ps/nm/km,

-9.95 ps/nm/km, -24.47 ps/nm/km, respectively.

To realize a MIR SC evolution with a pulse duration of 100-fs, the all-normal dispersion SC simulation is performed by launching a fundamental mode of secant pulse into the 10-mm-long optimized TCF with the largest input power of 3 kW. For the TCF with a side length of 5.5 μm, a broadband MIR SC extending from 2.5 to around 7 μm could be generated containing some minor spectral fluctuation around the pump wavelength as shown in solid black line in Fig. 9(a). The other two TCF designs with side length of 5 and 4.5 μm are optimized in such a way that the GVD parameters at the pump wavelength become lowered (dotted red and dashed blue curves in Fig. 2(b)) which significantly reduces the spectral fluctuation around the pump source as can be seen in Fig. 9(b) and 9(c) (dotted red and dashed blue lines), respectively. The predicted SC evolution extending up to 6.2 μm and 5.8 μm are achieved by these two structures. However, SC bandwidth at the TCF output somewhat decreases, eventually increasing spectral flatness by reducing fluctuations among spectral components over the entire SC bandwidth.
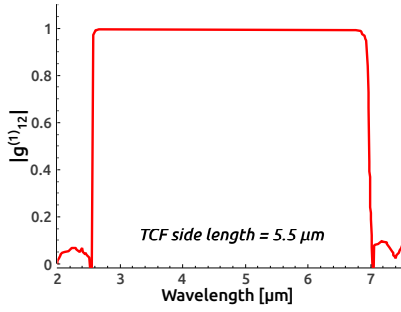
Fig. 10. First-order coherence simulated over the entire SC bandwidth for the TCF geometry containing side length $a = 5.5\ \mu m$ corresponding to the Figs. 9(a), 9(d) and 9(g) (entire left column), respectively.

Spectral densities (middle row) and spectrograms (bottom row) are given in Fig. 9, corresponding to all-normal dispersion SC spectra obtained in Fig. 9 (top row) to show how the SC spectra evolves along the length of the optimized 10-mm-long TCF design. As mentioned earlier, SC evolution in all-normal dispersion pumping is mainly dominated initially by SPM and later by OWB. In the case of all-normal dispersion SC evolution, one has to initially observe the symmetrical spectral extension around the pump wavelength due to SPM when an ultra short pulse launches into the TCF structure. Later, an overlap occurs among different frequency components owing to the longer wavelength components propagating faster than their shorter wavelength counterparts. In the temporal domain, the OWB results in the overlap of two pulse components generates new frequency components, creating the two side lobs in the blue and red wavelength component sides of the SC spectra as can be seen in both spectral density evolutions and spectrograms of Fig. 9 (top and bottom rows, respectively).

Finally, the coherence of the output of all-normal dispersion SC spectra obtained for a TCF structure containing side length $a = 5.5\ \mu m$ from an ensemble average is calculated using Eq. (7) from twenty independently simulated SC spectra pairs. For coherence calculation, the input pump pulse is increased by adding random noise with 1% of the pulse intensity during all-normal dispersion SC simulations. Figure 10 shows the modulus of complex degree of first-order coherence $|g_{12}^{(1)}(\lambda)| = 1$ which implies the SC output is highly coherent over the entire bandwidth for this design. Similar results are obtained for the remaining two TCF geometries optimized for pumping in all-normal dispersion region as well.

CONCLUSION

In this work, a 10-mm-long dispersion engineered all-chalcogenide triangular core microstructured fiber for MIR SC generation from the anomalous dispersion pumping to normal dispersion pumping region is proposed and simulated. In the case of anomalous dispersion pumping, three TCF geometries are optimized by varying their side length for pumping at a wavelength of $4\ \mu m$. An ultrabroadband MIR SC spectral evolution covering the wavelength range 2.2-13.5 μm could be generated by the optimized TCF structure containing side length of $7\ \mu m$. By increasing the side length to 7.5 μm, SC spectral evolution can be extended up to 15 μm. The bandwidth can further be enhanced beyond 15 μm by increasing the side length to $8\ \mu m$ by the proposed TCF design. In all cases, the largest low pump

peak power of 3 kW is used. This is the encouraging prediction by our design, however, bandwidth could somewhat actually be reduced owing to long wavelength cladding absorption at the TCF output.

For all-normal dispersion pumping, the TCF structure is optimized by varying its side length for broadband ultraflat SC generation in the MIR region. To investigate spectrum flatness, three different designs have been proposed depending on its side length variation between 5.5 μm and 4.5 μm. It has been observed from these designs that the SC spectra can be spanned up to $7\ \mu m$ in the MIR region by using a TCF structure containing side length of 5.5 μm. Slight spectral fluctuation can be observed between both side of the pump source by this design. The spectral flatness can be improved by reducing the side-length, which eventually reduces bandwidth slightly at the TCF output.

The two different all-chalcogenide novel TCFs proposed and modelled for operation in the anomalous and all-normal dispersion MIR region SC generation can be used in molecular fingerprint spectroscopy, atmospheric gas sensing, biomedical imaging as well as many more fiber based broadband applications.

REFERENCES

1. A. Schliesser, N. Picque, and T. W. Haensch, "Mid-infrared frequency combs," Nat. Photonics **6**, 440–449 (2012).
2. M. Michalska, J. Mikolajczyk, J. Wojtas, and J. Swiderski, "Mid-infrared, super-flat, supercontinuum generation covering the 2–5 μm spectral band using a fluoroindate fibre pumped with picosecond pulses," Sci. Reports **6**, 39138 (2016).
3. J. M. Dudley, G. Genty, and S. Coen, "Supercontinuum generation in photonic crystal fiber," Rev. Mod. Phys. **78**(4), 1135–1184 (2006).
4. B. J. Eggleton, B. Luther-Davies, and K. Richardson, "Chalcogenide photonics," Nat. Photonics **5**, 141–148 (2011).
5. T. Cheng, K. Nagasaka, T. H. Tuan, Xiaojie Xue, M. Matsumoto, H. Tezuka, T. Suzuki, and Y. Ohishi, "Mid-infrared supercontinuum generation spanning 2 to 15.1 μm in a chalcogenide step-index fiber," Opt. Lett. **41**, 2117-2120 (2016).
6. X. Gai, T. Han, A. Prasad, S. Madden, D. Y. Choi, R. Wang, D. Bulla, and B. Luther-Davies, "Progress in optical waveguides fabricated from chalcogenide glasses," Opt. Express **18**(25), 26635–26646 (2010).
7. Y. Yu, X. Gai, T. Wang, P. Ma, R. Wang, Z. Yang, D. Choi, S. Madden, and B. Luther-Davies, "Mid-infrared supercontinuum generation in chalcogenides," Opt. Mater. Express **3**(8) 1075–1086 (2013).
8. C. Markos, I. Kubat, and O. Bang, "Hybrid polymer photonic crystal fiber with integrated chalcogenide glass nanofilms," Sci. Reports **4**, 6057 (2014).
9. C. Wei, X. Zhu, R. A. Norwood, F. Seng, and N. Peyghambarian, "Numerical investigation on high power mid-infrared supercontinuum fiber lasers pumped at 3 μm," Opt. Express **21**(24), 29488–29504 (2013).
10. C. R. Petersen, U. Mφller, I. Kubat, B. Zhou, S. Dupont, J. Ramsay, T. Benson, S. Sujecki, M. Abdel-Moneim, Z. Tang, D. Furniss, A. Seddon, and O. Bang, "Mid-infrared supercontinuum covering the 1.4-13.3 μm molecular fingerprint region using ultra-high NA chalcogenide step-index fiber," Nat. Photonics **8**, 830–834 (2014).
11. Z. Zhao, B. Wu, X. Wang, Z. Pan, Z. Liu, P. Zhang, X. Shen, Q. Nie, S. Dai, and R. Wang, "Mid-infrared supercontinuum covering 2–16 μm in a low-loss telluride single-mode fiber," Laser Photonics Rev. **2**, 1700005 (2017).

12. C. R. Petersen, R. D. Engelsholm, C. Markos, L. Brilland, C. Caillaud, J. Troles, and O. Bang, "Increased mid-infrared supercontinuum bandwidth and average power by tapering large-mode-area chalcogenide photonic crystal fibers," Opt. Express **25**, 15336–15348 (2017).

13. D. D. Hudson, S. Antipov, L. Li, I. Alamgir, T. Hu, M. El-Amraoui, Y. Messaddeq, M. Rochette, S. D. Jackson, and A. Fuerbach, "Toward all-fiber supercontinuum spanning the mid-infrared," Optica **4**, 1163–1166 (2017).

14. U. Møller, Y. Yu, I. Kubat, C. R. Petersen, X. Gai, L. Brilland, D. Mechin, C. Caillaud, J. Troles, B. Luther-Davies, and O. Bang, "Multi-milliwatt mid-infrared supercontinuum generation in a suspended core chalcogenide fiber," Opt. Express **23**(3), 3282–3291 (2015).

15. Y. Yu, X. Gai, P. Ma, K. Vu, Z. Yang, R. Wang, D. Choi, S. Madden, and B. Luther-Davies, "Experimental demonstration of linearly polarized 2-10 μm supercontinuum generation in a chalcogenide rib waveguide," Opt. Lett. **41**(5), 958–961 (2016).

16. Z. Zhao, X. Wang, S. Dai, Z. Pan, S. Liu, L. Sun, P. Zhang, Z. Liu, Q. Nie, X. Shen, and R. Wang, "1.5-14 μm mid-infrared supercontinuum generation in a low-loss Te-based chalcogenide step-index fiber," Opt. Lett. **41**, 5222–5225 (2016).

17. Y. Yu, B. Zhang, X. Gai, C. Zhai, S. Qi, W. Guo, Z. Yang, R. Wang, D. Choi, S. Madden, and B. Luther-Davies, "1.8-10 μm mid-infrared supercontinuum generated in a step-index chalcogenide fiber using low peak pump power," Opt. Lett. **40**, 1081–1084 (2015).

18. C. R. Petersen, P. M. Moselund, C. Petersen, U. Møller, and O. Bang, "Spectral-temporal composition matters when cascading supercontinua into the mid-infrared," Opt. Express **24**, 749–758 (2016).

19. I. Kubat, C. S. Agger, U. Møller, A. B. Seddon, Z. Tang, S. Sujecki, T. M. Benson, D. Furniss, S. Lamrini, K. Scholle, P. Fuhrberg, B. Napier, M. Farries, J. Ward, P. M. Moselund, and O. Bang, "Mid-infrared supercontinuum generation to 12.5 μm in large NA chalcogenide step-index fibres pumped at 4.5 μm," Opt. Express **22**, 19169–19182 (2014).

20. M. R. Karim, B. M. A. Rahman, and G. P. Agrawal, "Mid-infrared supercontinuum generation using dispersion-engineered Ge$_{11.5}$As$_{24}$Se$_{64.5}$ chalcogenide channel waveguide," Opt. Express **23**(5), 6903–6914 (2015).

21. T. S. Saini, A. Kumar, and R. K. Sinha, "Broadband mid-infrared supercontinuum spectra spanning 2-15 μm using As$_2$Se$_3$ chalcogenide glass triangular-core graded-index photonic crystal fiber," J. Lightw. Technol. **33**(18), 3914–3920 (2015).

22. I. Kubat, C.R. Petersen, U. Møller, A. Seddon, T. Benson, L. Brilland, D. Mechin, P.M. Moselund, and O. Bang, "Thulium pumped mid-infrared 0.9-9 μm supercontinuum generation in concatenated fluoride and chalcogenide glass fibers," Opt. Express **22**, 3959–3967 (2014).

23. M. R. Karim, B. M. A. Rahman, Y. O. Azabi, A. Agrawal, and G. P. Agrawal, "Ultra-broadband mid-infrared supercontinuum generation through dispersion engineering of chalcogenide microstructured fibers," J. Opt. Soc. Am. B **32**(11), 2343–2351 (2015).

24. P. Ma, D. Y. Choi, Y. Yu, X. Gai, Z. Yang, S. Debbarma, S. Madden, and B. Luther-Davies, "Low-loss chalcogenide waveguides for chemical sensing in the mid-infrared," Opt. Express **21**(24), 29927–29937 (2013).

25. B. M. A. Rahman and J. B. Davies, "Finite-element solution of integrated optical waveguides," J. Lightw. Technol. **2**, 682–688 (1984).

26. G. P. Agrawal, Nonlinear Fiber Optics 5th ed. (Academic, San Diego, California, 2013).

27. X. Gai, S. Madden, D. Y. Choi, D. Bulla, and B. Luther-Davies, "Dispersion engineered Ge$_{11.5}$As$_{24}$Se$_{64.5}$ nanowires with a nonlinear parameter of 136 W^{-1}m^{-1} at 1550 nm," Opt. Express **18**(18), 18866–18874 (2010).

28. M. R. Karim and B. M. A. Rahman, "Ultra-broadband mid-infrared supercontinuum generation using chalcogenide rib waveguide," Opt. Quant. Electron. **48**(3), 174 (2016).

29. V. V. R. K. Kumar, A. K. George, W. H. Reeves, J. C. Knight, P. St. J. Russell, F. G. Omenetto, and A. J. Taylor, "Extruded soft glass photonic crystal fiber for ultrabroad supercontinuum generation," Opt. Express **10**, 1520–1525 (2002).

30. T. Wang, X. Gai, W. Wei, R. Wang, Z. Yang, X. Shen, S. Madden, and B. Luther-Davies, "Systematic z-scan measurements of the third order nonlinearity of chalcogenide glasses," Opt. Mater. Express **4**(5), 1011–1022 (2014).

31. A. Al-Kadry, L. Li, M. E. Amraoui, T. North, Y. Messaddeq, and M. Rochette, "Broadband supercontinuum generation in all-normal dispersion chalcogenide nanowires," Opt. Lett. **40**(20), 4687–4690 (2015).

32. B. Siwicki, M. Klimczak, R. Stepien, and R. Buczynski, "Supercontinuum generation enhancement in all-solid all-normal dispersion soft glass photonic crystal fiber pumped at 1550 nm," Opt. Fiber Tech. **25**, 64–71 (2015).

33. L. Liu, T. Cheng, K. Nagasaka, H. Tong, G. Qin, T. Suzuki, and Y. Ohishi, "Coherent mid-infrared supercontinuum generation in all-solid chalcogenide microstructured fibers with all-normal dispersion," Opt. Lett. **41**(2), 392–395 (2016).

34. G. Stepniewski, M. Klimczak, H. Bookey, B. Siwicki, D. Pysz, R. Stepien, A. K. Kar, A. J. Waddie, M. R. Taghizadeh, and R. Buczynski, "Broadband supercontinuum generation in normal dispersion all-solid photonic crystal fiber pumped near 1300 nm," Laser Phys. Lett. **11**, 055103 (2014).

35. Z. Guo, J. Yuan, C. Yu, X. Sang, K. Wang, B. Yan, L. Li, S. Kang, and X. Kang, "Highly coherent supercontinuum generation in the normal dispersion liquid-core photonic crystal fiber," Prog. in Elec. Res. **48**, 67–76 (2016).

36. M. R. Karim, H. Ahmad, and B. M. A. Rahman: "All-normal-dispersion chalcogenide waveguides for ultraflat supercontinuum generation in the mid-infrared region", IEEE J. Quan. Elec. **53**(2) (2017).

37. A. B. Salem, R. Cherif, and M. Zghal, "Raman response of a highly nonlinear As$_2$Se$_3$-based chalcogenide photonic crystal fiber," Proc. PIERS, Morocco, 1256 (2011).

38. X. Gu, M. Kimmel, A. P. Shreenath, R. Trebino, J. M. Dudley, S. Coen, and R. S. Windeler, Experimental studies of the coherence of microstructure-fiber supercontinuum, Opt. Express **11**(21), 2697-2703 (2003).

39. Y. Yu, B. Zhang, X. Gai, P. Ma, D. Choi, Z. Yang, R. Wang, S. Debbarma, S. J. Madden, and B. Luther-Davies, "A broadband, quasi-continuous, mid-infrared supercontinuum generated in a chalcogenide glass waveguide," Laser Photonics Rev., 1–7 (2014).

40. Y. Tang, L. G. Wright, K. Charan, T. Wang, C. Xu, and F. W. Wise, "Generation of intense 100-fs solitons tunable from 2 to 4.3 μm in fluoride fiber," Optica **3**, 948-951 (2016).

41. M. R. Karim, B. M. A. Rahman, and G. P. Agrawal, "Dispersion engineered Ge$_{11.5}$As$_{24}$Se$_{64.5}$ nanowire for supercontinuum generation: A parametric study," Opt. Express **22**(25), 31029–31040 (2014).

42. P. Falk, M. H. Frosz, and O. Bang, "Supercontinuum generation in a photonic crystal fiber with two zero-dispersion wavelengths tapered to normal dispersion at all wavelengths," Opt. Express **13**(19), 7535–7540 (2005).

43. A. M. Heidt "Pulse preserving flat-top supercontinuum generation in all-normal dispersion photonic crystal fibers," J. Opt. Soc. Am. B **27**(3), 550–559 (2010).

44. A. M. Heidt, A. Hartung, G. W. Bosman, P. Krok, E. G. Rohwer, H. Schwoerer, and H. Bartelt, "Coherent octave spanning near-infrared and visible supercontinuum generation in all-normal dispersion photonic crystal fibers," Opt. Express **19**(4), 3775–3778 (2011).

45. C. Finot, B. Kibler, L. Provost, and S. Wabnitz, "Beneficial impact of wave-breaking for coherent continuum formation in normally dispersive nonlinear fibers," J. Opt. Soc. Am. B **25**(11), 1938–1337 (2008).

46. A. Hartung, A. M. Heidt, and H. Bartelt, "Design of all-normal dispersion microstructured optical fibers for pulse-preserving supercontinuum generation," Opt. Express **19**(8), 7742-7749 (2011).

47. L. E. Hooper, P. J. Mosley, A. C. Muir, W. J. Wadsworth, and J. C. Knight, "Coherent supercontinuum generation in photonic crystal fiber with all-normal group velocity dispersion," Opt. Express **19**(6), 4902–4907 (2011).